VIII. POTASSIUM RANKINE SYSTEMS TECHNOLOGY

Robert E. English, Robert L. Cummings, Robert L. Davies,
Thomas P. Moffitt, and Uwe H. von Glahn

INTRODUCTION

The type of potassium Rankine system considered (fig. VIII-1) in this paper contains four fluid loops, namely, a reactor loop, a power loop, a heat-rejection loop, and a cooling loop. The basis for system operation is like that of SNAP-8, the main differences being that here the temperatures are higher and that potassium rather than mercury is used in the power loop. The particular temperatures shown illustrate the levels that might be used; these temperatures, although high, are within the capabilities of the alloy T-111 discussed in paper VII. The reactor outlet temperature is taken to be 2200° F. The reactor coolant will drop 100° or 200° in passing through the potassium boiler and will be heated an equal amount in the reactor.

One of the main reasons for use of a separate loop for the reactor is to diminish the problems of shielding against nuclear radiation. If some of the reactor fuel elements develop small cracks, the reactor might well be capable of continued operation, but some fission products could then leak into the reactor coolant stream. In the case of the separate reactor loop, as shown in figure VIII-1, the resulting increased radioactivity would be confined to the reactor, the boiler, and the pump in the reactor loop. If a separate reactor coolant loop were not used, this radioactivity would contaminate the entire power loop, thereby complicating the problems of shielding, inspection, and maintenance of the power system.

At the turbine inlet, the potassium vapor can be superheated somewhat. In general, the boiling temperature will be approximately equal to the temperature at the reactor inlet, and the resulting vapor can be superheated to nearly the temperature at the reactor outlet. In this way, the amount of superheat at the turbine inlet might typically be 50° to 150° F.

The condensing and radiating functions are separated for two reasons. First, the design calculations indicate that system weight is thereby diminished. And second, the design of the power loop is then almost independent of the manner in which the power system integrates with the spacecraft and mission. Radiator geometry can be adapted to each spacecraft and mission with only minor alterations in pumping power. The fourth, or cooling, loop provides low-temperature coolant to those system components that require it.

Such a system has a considerable number of components and a substantial diversity of the problems. The program has so far been an investigation of the various constituent problems of these several components, that is, the general technology of such a power system. For this reason, the following discussion covers a variety of problems that are seemingly independent. The characteristic that ties all these problems together is that they must all be solved in order for such a system as this to function.

In the following discussion, various constituent problems are treated successively. For a period of time, the reactor problems were investigated by Pratt & Whitney CANEL in an AEC sponsored program. More recently, the responsibility for space-power reactors was transferred to the Livermore laboratory, thus the reactor program is presently in the formative stage. Additional study is required before the reactor concept is selected; for this reason, the reactor is not discussed.

BOILER AND CONDENSER

To obtain good performance of the boiler and the condenser in a Rankine cycle space-power system, the heat-transfer processes associated with two-phase flow of liquid metals must be understood. To obtain an efficient and reliable power system, stable operation of these two components must be obtained, both by themselves and by their interactions with other parts of the system.

Boiler

Study of two-phase flow problems with liquid metals has been aided greatly by parallel studies with conventional fluids, such as Freon and water. Thus, the results of heat transfer and pressure drop research with conventional fluids in relatively inexpensive rigs can be applied to liquid-metal systems by considering the pertinent physical properties of each fluid. Furthermore, the conditioning problem encountered with the SNAP-8 mercury system does not exist with alkali metals because of their excellent wetting characteristics, as well as the great care taken to keep alkali metal systems clean and free of contamination. Analysis of experimental liquid-metal data has shown that the two-phase heat-transfer resistance is generally very low.

Typical data obtained with a single-tube heat-exchanger boiler with potassium as the working fluid are shown in figure VIII-2, where the boiler thermal resistance is plotted as a function of boiler exit quality and superheat. The boiler thermal resistance is used instead of its reciprocal, the heat-transfer coefficient, because resistances can be added to each other directly. The thermal resistance of the boiler is made up of the following three resistances: the heating fluid, the tube wall, and the boiling fluid. The heating-fluid resistance and the tube-wall resistance can be readily calculated and are shown by the crosshatched regions in the figure. The boiling resistance is then determined from the difference between the sum of these two calculated resistances and the measured overall values shown by the data points. For the most part, the boiling-fluid resistance is much less than the sum of that for the wall and heating fluid and, therefore, is not the controlling thermal resistance in a liquid-metal boiler. Only in the region of very low quality, and again at vapor superheat, is the boiling-fluid resistance of a magnitude that might be considered controlling. The low values of boiling-fluid thermal resistance obtained for these data represent very high boiling heat-transfer coefficients, generally in the range of 8000 to 30 000 Btu per hour per square foot per $^{\circ}F$.

From these and other studies, it can be concluded that the heat transfer and associated pressure drops for liquid-metal boilers present no serious problems for designers. Then what does constitute the problem area for boilers?

The main area of concern is stable operation of a system that includes two-phase flow in some of the components, and, in particular, the boiler. A system is stable if, when it is disturbed from its operating point, it inherently returns to the same point. The stability of the system depends not only on the stability of each of the components, but on the manner in which the components interact. Although two-phase components may be stable by themselves, component interactions may cause the system to become unstable. Stable operation of two-phase components, therefore, is as much a system problem as it is a component design problem.

Boiler stability problems are many and complex. Two primary problem areas are described: the flow patterns that may exist in a boiler tube, and the "negative-resistance" characteristic of a boiler.

The complicated flow patterns that result from forced-convection boiling within a hollow-tube boiler are shown in figure VIII-3. The boiling fluid flows within a tube and is heated by a second fluid that moves in a surrounding shell. At the beginning of the boiler tube, the fluid is all-liquid and at a temperature below the boiling point (the saturation temperature). The graph in the lower part of the figure illustrates the heating flux being transferred into the boiler tube. In the all-liquid region, the heat transfer is relatively low, since it occurs by ordinary forced convection. As the liquid is heated, the portion near the wall reaches the boiling point. Bubbles are then formed near the wall with the core of the fluid remaining liquid. Here the heat transfer begins to increase because of the boiling action. The bubbly flow regime is reached when the core of the liquid approaches the boiling point and bubbles extend over the entire tube cross section. These bubbles then coalesce, forming large vapor masses. The result is the slug-flow regime, with the flow alternating rapidly between liquid and vapor. Liquid is still flowing along the wall and the heat transfer is very high. The vapor slugs then merge together and annular flow results, where an annulus of liquid flows along the wall and vapor flows at high velocity down the center of the tube. The last regime is mist flow, where the wall is essentially dry and vapor is carrying entrained liquid droplets. Somewhere prior to the region of a dry wall, the heat transfer experiences a transition and very abruptly decreases to a low heat flux rate. This transition point may fluctuate up and down the tube in a rapid, uncontrolled manner.

A number of inherent boiler stability problems are tied to these flow regimes. The slug-flow regime is inherently very unstable and causes violent surges in pressure and flow. These surges are believed to be largely responsible for the fluctuations in the heat-transfer transition point that occurs further downstream in the tube.

Another instability occurs at the very start of the boiling process. The initiation of boiling in liquid metals is erratic because of a bubble-nucleation problem. While most liquids begin to boil when heated only a few degrees above their normal boiling temperature, liquid metals can be heated to several hundreds of degrees above their normal boiling temperature and still remain entirely liquid. Then, at some point, the liquid in the boiler will suddenly break to form an interface and flash into vapor. Flash vaporization results in a sudden release of energy that causes violent bumping, geysering, and water hammer in the fluid. The outrush of vapor may send a surge of flow and pressure around the power conversion loop, thereby forcing cooler liquid back into the boiler tube, refilling the tube with liquid and setting up another superheating and geysering cycle.

The highly superheated liquid state that can be obtained with alkali metals is caused by conditions that are unfavorable for bubble formation. Studies have shown that bubbles originate at gas- or vapor-filled cavities or nucleation sites, such as pits and scratches in the boiler-tube surface. Under such conditions, boiling can be initiated and maintained with only a few degrees of superheat. With alkali metals, however, the systems are highly degassed to help reduce corrosion and oxidation, thus depleting the gas available at the nucleation sites. Also, these fluids wet the surface exceedingly well, thereby tending to fill many of the larger cavities and render them inactive. These combined effects are the primary cause of the bubble-nucleation problem with liquid metals.

In addition to these flow-pattern instabilities, a forced-flow boiler has, in general, a "negative-resistance" characteristic in its operating range. Some data that illustrate the negative-resistance characteristic of a boiler are shown in figure VIII-4. Here, the pressure drop for a hollow boiler tube is plotted as a function of the weight flow of the fluid. While the data shown are for sodium, similar data are obtained with other fluids. The solid lines show the pressure drops for all-vapor and all-liquid flows, while the dot-dash parallel lines between these limits represent nominal exit vapor quality values. A negative resistance is characterized by a decrease in pressure drop with increasing flow, that is, a negative slope of the curve. The slope of the curve can become negative because an increase in total flow results in a decrease in exit quality, and, hence, a decrease in vapor velocity and pressure drop.

On the negative slope portion of the curve, any flow disturbance tending to increase the flow would lead to a reduction in pressure drop, which, in turn, would cause a further increase in flow rate. An increased flow rate creates an unstable region of boiler operation that leads, in many cases, to severe boiler and system instabilities. The magnitude and location of this negative slope are a function of many variables including liquid subcooling, heat input, fluid pressure level, boiler internal configuration, etc. Thus, a whole family of such curves can be generated to cover the operating range of a particular boiler tube.

It is important to realize that the region of negative slope does not necessarily indicate that the boiler is unstable in this operating range, but does indicate that, when the boiler is coupled with an unsuitable feed-system resistance, an energy source exists which could become a driving force for a system instability.

The negative slope of the boiler operating curve (fig. VIII-4), discussed previously, can be eliminated by adding a high-resistance device at the inlet of each boiler tube. An orifice (fig. VIII-5), whose pressure drop increases with the square of the weight flow, has frequently been used for this purpose. The overall boiler pressure drop is then made up of the sum of the boiler-tube and orifice pressure drops. This combined pressure drop of the sodium boiler tube and an orifice is shown in figure VIII-6 as a function of weight flow. It is apparent that the combined pressure-drop curve has only a positive slope and thus the negative-resistance characteristic of the boiler tube has been eliminated as an instability source. An orifice, being a high-resistance element, also tends to decouple the boiler from disturbances originating upstream in other components. By itself, however, an orifice at the boiler inlet does not solve the slug-flow and the bubble-initiation problems.

Of the various inlet devices presently being used for space boiler applications, the central plug and helical spring shown in figure VIII-7 merit discussion. In this configuration, the plug, by reducing the flow area, increases the liquid velocity and thus enhances the heat transfer, while the spiral flow path moderates the slug flow by centrifuging the heavier liquid to the wall of the tube. With this device, however, the point of initiation of boiling is uncertain, and slug flow, depending on the operating conditions, may or may not occur. The device does not by itself solve the bubble-initiation problem; however, artificial nucleation sites in the form of re-entrant cavities could circumvent this shortcoming.

An advanced technique that attempts to solve all the previously discussed instability problems is shown in figure VIII-8. At the top of the figure, a schematic drawing of the proposed boiler-tube inserts is shown. The inserts consist of a small center-tube device at the boiler inlet followed by a helical spring. The lower portion of the figure shows a photograph of a transparent tube test section in which hot water was used to study the flow patterns obtained with these inserts. The flow patterns obtained with these inserts are shown in more detail by the use of close-up photographs. Upstream of the small center tube (fig. VIII-9), the flow is all liquid. The center tube creates a significant pressure drop near the tube outlet where the incoming liquid approaches its saturation or boiling temperature and then provides a spray-type, flashing discharge. The vaporization of a small portion of the flow by flashing provides the vapor required to initiate boiling, and thereby eliminates the bubble-nucleation problem. Furtheremore, since the flashing location is fixed by the center-tube outlet, initiation of boiling is fixed and known. Downstream of the spray (fig. VIII-10), an annular flow pattern is quickly established, with the liquid spiraling along the tube wall and the vapor flowing down the center of the tube. The liquid-vapor interface is wavy but apparently unbroken.

In summary, a center-tube insert should eliminate the bubbly and slug-flow regimes entirely, decouple the upstream feed components, provide positive resistance, and forcibly initiate boiling at a fixed location with a prescribed flow regime.

At the boiler-tube outlet it is desirable to provide droplet-free vapor with vapor superheat of the order of 100° F to ease turbine operating problems. To provide for droplet-free, superheated vapor, boiler tubes can be designed to centrifuge the heavier droplets in the mist flow regime to the tube walls. Typical inserts that have been used to accomplish this include twisted tapes, spiral ribbons, and helical springs, as shown in previous figures.

Representative heat-transfer data for a potassium boiler tube illustrating the effectiveness of such a device in achieving vapor superheat are shown in figure VIII-11 as a function of vapor quality and superheat. Data are shown for a hollow tube and for a twisted tape insert. With a hollow tube, a quality of less than 90 percent could be achieved. Use of a twisted tape with a pitch-to-diameter ratio of 2 resulted in a vapor superheat of about 200° F. The heat-transfer coefficient in the midquality region was roughly the same for the two configurations.

Of the high-quality region inserts, the helical spring appears to be most advantageous because liquid drops have no opportunity to stream along a surface that extends to the center of the tube, as has been observed with twisted tapes. Curving the boiler tube, such as in the SNAP-50 boiler design, will also aid in separating the two phases. All the inserts, however, penalize the system by increasing the pressure drop for the boiler, generally by a factor of 2 or more over that for a hollow tube.

Stability studies of two-phase components, particularly boilers, have historically been hampered by lack of dynamic data with which to evaluate mathematical models and analyses. Lewis has begun research in component and system dynamics with water and Freon as convenient working fluids. Briefly, the technique used in this research consists of varying by a small amount a parameter such as weight flow, sinusoidally over a range of frequencies. The response of one variable with respect to another can be obtained solely in terms of frequency. Comparison with analytical models then allows possible sources of instability to be pinpointed. Considerably more experimental data are needed before generalized models of two-phase dynamic behavior can be developed and verified.

Condenser

In general, more is known about the condenser than about the boiler. Successful operation of both convectively cooled and radiantly cooled multitube potassium condensers has been achieved over a range of vapor temperatures that exceeds the 1350° F called for in figure VIII-1. No serious instabilities were encountered over the wide range of operating conditions covered, even when the pressure drop across the units was essentially zero.

Views of the seven-tube, convectively cooled, potassium condenser are shown in figure VIII-12. The condenser was of a "hockey stick" design to facilitate thermal expansion and was 72 inches long. The condenser was made of 316 stainless steel. NaK was used as the coolant fluid, and flowed countercurrent in the shell. Data were obtained up to 1500° F.

Temperature profiles of both the condensing fluid and coolant shell for one run are shown in figure VIII-13 as a function of distance downstream from the vapor inlet. The vapor (flowing from left to right) entered the condenser at 1400° F with an inlet quality of 86 percent. The pressure drop, and hence the saturation temperature change, was negligible for these data. Thus, the temperature of the condensing vapor can be assumed to remain constant at the inlet value until the vapor is completely condensed, indicated as the interface in the figure. Thereafter, the condensed fluid temperature subcools rapidly, reaching substantially the temperature of the coolant shell within a few inches downstream from the interface.

The coolant fluid, flowing countercurrent to the condensing fluid (right to left in the figure), enters the condenser at 1284° F. The shell temperature is substantially constant at this value until the interface is reached, then it increases as condensing occurs, reaching a value of 1348° F at the coolant flow outlet.

Typical coolant-shell temperature profiles for various coolant inlet temperatures are shown in figure VIII-14 again as a function of length from the vapor inlet. These data were obtained with constant inlet conditions (1400° F inlet vapor temperature), a constant coolant flow rate, and a measured pressure drop across the condenser of less than 1 pound per square inch. The vapor temperature profiles are not shown. They are similar to those discussed in figure VIII-13, namely, constant temperature of 1400° F during condensing and temperature approaching that of the coolant just downstream from the liquid-vapor interface. The locations of the liquid-vapor interfaces are indicated by the arrows. The condensing length, measured from the vapor inlet, increases rapidly with increases in coolant inlet temperature, changing from $9\frac{1}{2}$ to 44 inches for a change in the coolant inlet temperature from 1194° to 1304° F. With a coolant inlet temperature of 1315° F, complete condensing of the vapor was not obtained in the 72-inch length of the condenser.

The two lower curves (fig. VIII-14) represent typical data for high heat flux values near the vapor inlet. The condensing lengths for these two conditions, in which large temperature differences between the vapor and coolant fluid exist, can be predicted by very simple analyses. On the other hand, the two upper curves indicate a near absence of heat transfer (low heat flux) near the vapor inlet due to the small temperature difference between the vapor and coolant. The condensing lengths obtained with small vapor-to-coolant temperature differences cannot, as yet, be predicted. The problem is that the local pressure, and hence local vapor saturation temperature, in the entrance region of the condenser tubes cannot be accurately predicted for the prevailing two-phase flow. Thus, an accurate vapor-to-coolant temperature difference cannot be calculated when small differences are involved with the result that significant errors in calculated condensing lengths can be made.

TURBINE

Turbine-Rotor Materials

The materials problems in the turbine rotor are substantially different from those of just containing liquid potassium as discussed in paper VII. In particular, there is very little liquid potassium in the turbine, the turbine rotor is highly stressed because of its high rotational speed, and the turbine rotor is not required to have the same levels of ductility and weldability as does most of the power system. Materials having high density such as tantalum would increase the stress on a rotating component. Hence, there has been an increased emphasis on materials of lower density, such as molybdenum and columbium.

The high stress in the turbine rotor is an item of concern because high stress produces creep. For highest efficiency, potassium turbines are designed with small operating clearances. Therefore, to maintain the original clearances, the selected material must undergo only small amounts of creep during the life of the turbine at the elevated operating temperature.

Thus, alloys for this application are usually the most creep resistant that can be fabricated from a particular alloy base. In general, the alloy must be forgeable and exhibit some ductility; generally, 5 or 6 percent elongation at room temperature will suffice. Other important requirements include corrosion and erosion resistance.

In the selection of materials for high creep strength, many alloys were screened in high-temperature creep tests in high vacuums. In figure VIII-15, creep data are shown for the molybdenum base alloy TZC, which was the most creep resistant of the candidate turbine materials. The figure illustrates the creep as a function of time at three different stresses and temperatures. After 10 000 hours, an applied stress of 20 000 pounds per square inch at 2000° F results in

0.5 percent creep, 19 000 pounds per square inch at 2056° F leads to 0.25 percent creep, and 25 000 pounds per square inch at 1856° F gives 0.18 percent creep.

It is also desirable and important that allowable stress to limit creep to a low value be predictable for other temperatures and times. In figure VIII-16, the data are presented in terms of stress as a function of the Larson-Miller parameter, which relates temperature and time to stress for a given percentage creep, in this case, 0.5 percent creep.

Of the several alloys that have been considered as turbine rotor materials, three are presented in this plot: the previously discussed TZC, a columbium alloy Cb-132M, and the molybdenum base TZM. Typical allowable stresses for 0.5 percent creep for TZC in 10 000 hours are 20 000 pounds per square inch at 2000° F and 30 000 pounds per square inch at 1800° F. The strength of the columbium alloy Cb-132M degrades more rapidly at high temperature than TZM and TZC.

A turbine material must also be resistant to corrosive attack by potassium vapor. Figure VIII-17 shows the results of a 5000-hour test in potassium vapor at 2000° F. The TZM alloy was tested in the form of segmented ring inserts located internally in the columbium - 1-percent-zirconium capsule. From the microstructures shown, no attack occurred as evidenced by the smooth surface of both the inside and outside diameters of the ring segment and the lack of any penetration either at the surface or at the grain boundaries. Also, the weight change in the five segments tested was less than 0.07 percent of the total weight. From this test and other supporting investigations, it is believed that the stronger molybdenum alloy TZC will also be compatible with the potassium vapor since there are only minor changes in composition from the TZM.

Potassium Expansion Process

The expansion of potassium vapor through the turbine is similar to the expansion of steam. When the expansion takes place in the wet vapor region, the question arises as to where condensation takes place initially. In addition, potassium vapor is composed of both monatomic and diatomic species, the amount of each varying with temperature. When the vapor expands through the turbine with decreasing temperature, the proportion of monatomic to diatomic vapor could change. This poses an additional question as to the type of nozzle expansion process experienced by potassium. A knowledge of this process is required to size the flow passages within the turbine. It is this sizing that determines the pressure distribution and work split between the turbine stages.

Consequently, nozzle expansion data have been accumulated for initially saturated vapors at temperatures to 1600° F. Although not a perfect gas, it was determined that, for practical purposes, the expansion follows the polytropic process equation $pv^n = c$. The value of the exponent n fell between 1.4 and 1.5. For the temperature range considered, condensation did not take place before the throat, or minimum area, of the nozzle. Independent measurements of pressure distribution and weight flow indicate that both flow and pressure distribution are predictable for potassium turbines.

Two-Stage Potassium Turbine Test

Description. - A two-stage turbine was fabricated and tested under contract by the General Electric Company. Figure VIII-18 is a photograph of the rotor prior to testing. The diameter of this rotor is about 10 inches. The buckets were constructed of the nickel-base alloy Udimet 700. Figure VIII-19 shows a partial assembly of the turbine with the rotors installed. Two types of tests were conducted, namely, a short-time performance test to determine blade performance, and an endurance test to determine the erosion characteristics of the turbine.

Performance. - For the performance test, potassium vapor was used at an inlet temperature of 1550° F. The inlet vapor was essentially saturated, in that the inlet quality was considered to be 99.5 percent. Figure VIII-20 presents the performance results in terms of static efficiency as a function of turbine pressure ratio for a constant speed of about 19 000 rpm. The solid curve was predicted prior to testing by using standard gas turbine practice and perturbing the results for moisture effects. At design pressure ratio the efficiency is seen to be approximately 70 percent. The experimental trend at off-design conditions follows closely the predicted curve. In general, then, there appears to be no particular problem in predicting the performance of potassium turbines.

Endurance. - The potassium turbine operating conditions for the endurance test are as follows:

First stage:	
Inlet temperature, °F	1500
Inlet quality, percent	99.5
Second stage:	
Inlet temperature, °F	1390
Inlet quality, percent	96.7
Tip speed, ft/sec	770
Exit:	
Temperature, °F	1260
Quality, percent	92.5

As the vapor expands through the turbine, both temperature and quality decrease. The lowest quality (or highest moisture) and maximum blade speed occur in the second stage. If erosion takes place, it would be expected to show up on the second-stage wheel. Tip speed is shown rather than rotative speed because it is indicative of the impact velocity between the heavy drops of liquid traveling at relatively low speed and the wheel buckets. Eight of the Udimet 700 nickel buckets were removed from the second-stage wheel and replaced with molybdenum-base buckets, four each of TZM and TZC. The turbine was then assembled and the endurance test begun. Data taken periodically throughout the test showed that the turbine performance remained constant.

The endurance test was interrupted at the end of 2000 hours, and the turbine was dismantled. Figure VIII-21 is a photograph of the second-stage wheel after 2000 hours of operation. The wheel was vapor blasted to remove small amounts of residual potassium that had clung to the surfaces. Little or no erosion resulted from the 2000-hour test. The leading edges and bucket tips were still sharp and retained their original shape. Some of the original machining marks were still visible. The buckets were then removed from the wheel and weighed. The average weight change of the buckets was as follows:

Material	Average change, percent
U-700	-0.019
TZM	-.105
TCZ	-.102

The loss in weight amounted to about 0.1 percent for the molybdenum specimens and even less for the nickel alloy. These minute changes in weight and the condition of the buckets led to the conclusion that erosion was not a factor for the given conditions of operation for any of these materials. The turbine was then reassembled, and the endurance test continued. When the total elapsed time amounted to about 4300 hours, the performance of the turbine remained unchanged, which would indicate that if any erosion had occurred, it had been tolerable.

Low Exit Quality

Recent experience has shown that a turbine exit quality of 93 percent, or a liquid content of 7 percent, results in negligible blade erosion. However, the cycle in figure VIII-1 results in a liquid content of 10 to 15 percent at the turbine exit. Whether or not this increased liquid content results in acceptable blade erosion has yet to be investigated. For this reason, the two-stage potassium turbine just discussed will be modified to have three stages. This three-stage turbine will be subjected to performance and endurance tests the same as those given the two-stage turbine. At the conclusion of the tests, it will be known more definitely if the desired liquid contents of 10 to 15 percent at the turbine exit are acceptable.

TURBOGENERATOR PROBLEMS

To obtain a satisfactory configuration for the potassium turbogenerator, the design constraints imposed by all its components must be considered. As shown in figure VIII-22, this unit will consist of four major parts, namely, (1) an axial-flow turbine with five to eight stages, (2) a solid-rotor inductor alternator with an externally cooled stator, (3) a set of bearings, and (4) the necessary seals.

Bearings and Seals

A number of different designs and arrangements can be chosen for each of these major components and, as a result, a number of different turbogenerator configurations are possible. These different approaches may be explained by referring to table VIII-1 where the designs that may be used for the lubricant system, the seals, and the generator are listed.

Because potassium vapor is passing through the turbine, it is natural to consider using liquid potassium as the lubricant in the bearings. Both the shaft bearings would thus be supplied with liquid potassium. Between the turbine rotor and the bearings a labyrinth seal would be required to separate the potassium vapor in the turbine from the liquid in the bearing cavity. If a similar seal is used between the bearings and the generator rotor, there would also be potassium vapor in the generator rotor cavity. Then a special seal would be required to keep the potassium out of the generator windings. The nature of this seal is discussed further later in the section Generator Materials.

It would also be possible to avoid the problems associated with potassium in the generator rotor cavity by venting this chamber to space vacuum. In this case, a potassium-to-space seal, such as the one described for mercury in the SNAP-8 system, will be required for the generator seals to prevent excessive loss of working fluid. Although there are complications associated with the potassium-space seal, this arrangement would have the major advantage of avoiding the possibility of potassium vapor damage to the generator stator.

Another design approach for the turbogenerator unit is to use oil as the lubricant for the bearings. If this approach is chosen, there will be oil in the bearing just adjacent to the turbine, and special precautions must be taken to avoid contamination of the potassium working fluid with the oil and also to avoid contamination of the oil with potassium. The seal between the turbine and the bearings would consequently consist of two seals, one seal between the potassium and the space vacuum, and another between the oil lubricant and the space vacuum. Such seals between oil and space vacuum have been developed for the SNAP-8 unit (see paper VI). This seal technology may also be utilized in the design of the potassium-space seal. With oil lubrication in the bearings, it is necessary to vent the generator rotor cavity to space vacuum in order to prevent oil vapor from coming into contact with the high-temperature rotor and stator parts and causing thermal decomposition of the oil vapor. An oil-to-space seal is therefore also required for the generator seal if oil lubrication is used.

Thus, the turbogenerator configuration will indeed be affected substantially by the choices made for its bearings and seals. There are two main approaches: for the first approach, conventional oil bearings and the space seal technology developed under the SNAP-8 program can be used (see paper VI). For the second approach, potassium-lubricated bearings with rotating space seals can be used, or a special static seal can be used to keep potassium out of the generator stator.

Liquid-Metal Bearing Experience

If potassium is chosen as the lubricant for the turbogenerator, fluid-film bearings will be used. In this type of bearing the load-carrying capacity is provided by pressures generated within the fluid film, and rolling, or rubbing, contact does not occur. Direct bearing material wear or fatigue is, therefore, not a problem. When potassium is used as a lubricant, these fluid-film bearings can also develop a large load-carrying capacity with a moderate bearing power consumption. The power loss for such bearings for a 300-kilowatt turbogenerator unit, for example, is not expected to exceed a few kilowatts. The potassium lubricated bearing is also well suited for high-temperature operation.

Now that the advantages have been described, the following questions remain to be answered:

(1) What are the problems for this type of bearing?

(2) What results are available to indicate selecting it for the space power system?

The problems that must be solved for a potassium-lubricated bearing for this use are as follows:

(1) Bearing instability must be avoided under the light loads associated with zero-gravity operation of the turbogenerator.

(2) Differential thermal expansion and housing distortion must be accommodated by special flexible or pivoting mounts.

(3) Materials are required that are compatible with high-temperature liquid metals.

These problems are the same in general as those for Brayton cycle turbomachinery discussed in paper V. This is indeed the case as shown by a comparison of the results. To solve the problem of obtaining stable liquid-metal bearings, numerous tests have been run at Lewis and other research centers on different bearing configurations. From those tests, the preloaded pivoted pad bearing (fig. VIII-23) is attractive. A tilting pad bearing, the cylindrical journal, and a pivot are shown at the bottom of the figure, and the assembled bearing with three pads installed is shown at the top. This bearing is the most stable type at very small applied loads since the tilting pad is inherently stabilizing. This type of bearing also has advantages for service in the high-temperature turbogenerator because the individual pads are self-alining and can correct for housing distortion.

Several types of full cylindrical bearings have also been investigated for liquid-metal use. This type of bearing employs different types of grooves and other modifications to obtain stable operation at light loads. Figure VIII-24 shows the herringbone groove bearing, which is a smooth cylindrical bearing with a journal containing herringbone grooves. This type has proved to be the most stable bearing in tests at Lewis. Other cylindrical-bearing configurations, however, have also been operated stably at high speed and light loads.

The bearing for use in the potassium turbogenerator must accommodate differential thermal expansion and housing thermal distortion. Figure VIII-25 therefore illustrates use of a flexible-mounting diaphragm to allow for differential motion of shaft and bearing. The pivots that provide bearing stability are also shown. This approach is the same as that used for the gas Brayton cycle system (paper V). If a full cylindrical bearing were used, a flexible mount to accommodate misalinement would also be needed.

A summary of the accomplishments of NASA and other agencies and their contractors shows that substantial experience has been accumulated with liquid-metal-lubricated bearings. Results obtained with a number of different fluids are as follows:

(1) Water has been used extensively to study the hydrodynamic characteristics of bearings, because water closely simulates liquid metals in this respect.

(2) For NaK, 3200 hours of endurance operation on pivoted-pad bearings has been achieved at 325° F. Additional tests were run on pressurized and hydrostatic journals in pumps at 1200° F.

(3) For sodium, high-speed tests were made at 800° F, and tests of the pivoted-pad and the herringbone-groove-type bearings showed the best stability. Low-speed tests have also been conducted for periods of 20 000 hours at temperatures up to 1100° F.

(4) Bearing tests have also been made on lithium to 800° F extending to 2100 hours.

(5) Potassium bearings have operated continuously for 1500 hours at temperatures to 600° F, and endurance tests on these bearings are presently continuing. Additional tests have been run at temperatures as high as 1200° F.

In the high-temperature sodium tests on pivoted-pad bearings, one possible problem encountered was the rapid pivot wear. A flexible-diaphragm mount has also been used for elimination of the pivots and thus elimination of the problem of pivot wear. This is a matter that will require continued investigation.

Bearing Materials

Not only must bearings be selected that are stable and that can accept the thermal transients of power system operation, but also bearing materials must be selected that are compatible with one another and with the alkali-metal lubricant. In selecting materials for liquid-metal-lubricated bearings, it is necessary first to see under what conditions the bearings must operate and what material properties will allow such operation. First, the bearings must operate in liquid metals, and thus corrosion resistance is required. Second, smooth lubricant flow passages are necessary; the material must be fabricated with a smooth surface that must be maintained. To maintain the surface, the material must resist abrasive damage; thus a high hardness is required. A high hardness of bearing materials has also been shown necessary in actual bearing tests.

Because the clearances in these bearings are very close, it is necessary for the materials to be dimensionally stable. Since the clearances are so small, a close match in thermal expansion between the bearing and shaft material is desirable since this would ease the design problems.

The last property to be considered here is the thermodynamic stability of the material. While dynamic stability is not a design requirement, it is a materials requirement because any elements transferred out of the material could ruin its structural integrity and make it unacceptable.

Many materials have been evaluated for this application, and table VIII-2 lists the properties that have been discussed, namely, coefficient of thermal expansion, Vickers hardness number, and material stability, both dimensional and thermodynamic. Three candidate bearing materials and two potential shaft materials are indicated. The bearing materials are titanium carbide - 10 columbium and two tungsten carbide materials, one bindered with a refractory metal and the other with cobalt. The shaft materials are the molybdenum base TZM and the cobalt-base Nivco.

The coefficient of thermal expansion, where a close match is desired, is shown for the materials; they do match well for the TZM and the tungsten carbide bearing materials, while there is some difference in the titanium carbide - 10 columbium. The Nivco is considerably different from all the other materials. Design studies are yet to be made on actual hardware to define what can be accomplished with these materials.

The Vickers hardness numbers for all the bearing materials have been measured and are quite high for the candidates in table VIII-2; thus they would be expected to resist abrasion. The dimensional stability of materials tested in potassium at 1200° F for 1000 hours was evaluated, and all the candidates had negligible changes.

A measure of thermodynamic stability is the amount of carbon transferred from the bearing material to a columbium - 1-percent-zirconium capsule. The carbon transfer was very low for all the materials tested at 1200° F. At 800° F, no transfer of carbon was observed for any of the materials listed. Corrosion resistance was evaluated in this test also, and there was no observed attack; this evaluation is based on visual, chemical, and metallographic examinations.

Generator Materials

The design features of an electrical generator for space applications are discussed in paper V. Just as for the Brayton system, the potassium Rankine generator will have a solid rotor. The differences are the higher operating temperature of the Rankine cycle generator and the possible presence of potassium vapor in the rotor cavity. Because of the meager information on electrical materials above 400° F, various candidate materials were tested in order to determine their electrical capabilities at high temperatures.

The cobalt-base alloy Nivco is a candidate rotor material. Nivco has a combination of high creep strength and acceptable magnetic properties. Figure VIII-26 shows creep curves for various temperatures and stresses. After 7000 hours at 1100° F with an applied stress of 37 500 pounds per square inch, Nivco has undergone only 0.8 percent creep. The creep curves provide design data in the 1100° F temperature range.

The next functional part of the generator to be considered is the stator. The laminations were made of the iron-base magnetic material Hyperco 27. Insulations were typically high-purity alumina except for that on the nickel-clad silver conductor. That insulation was Anadur-E glass plus refractory oxides, and the end-turn potting compound was phosphate-bonded zirconium silicate.

Figure VIII-27 shows a statorette constructed of the following electrical materials:

Component	Material
Magnetic material	Fe-27Co
Interlaminar insulation	Alumina
Slot insulation	Alumina
Electrical conductor	Nickel-clad silver
Conductor insulation	Anadur-E glass plus refractory oxides
Potting compound	Phosphate-bonded zirconium silicate

The assembly shown is representative of a 15-kilovolt-ampere 3-phase generator stator and has been tested in vacuum for 5000 hours with a hot-spot temperature of 1100° F. The photograph was taken after the 5000-hour test; the appearance of the assembly was unchanged by the test.

The properties measured were the conductor resistance and insulation resistance. Figure VIII-28 shows that the conductor resistance for the 5000-hour test was constant for the duration of test, which is indicative of material stability and lack of metallurgical interactions.

The insulation resistance (fig. VIII-29) was measured for both phase to phase and phase to ground. The resistance did not degrade; in fact, it actually improved. This improvement is the result of outgassing of water vapor and other volatile residuals that are being removed by the high vacuum.

Two solenoids and a transformer constructed of these same materials are shown in figure VIII-30. These units were tested in vacuum for 5000 hours with a hot-spot temperature of 1100° F. The two solenoids operated for 5000 hours, with one continuously energized and the other energized at 170-hour intervals to check for the occurrence of diffusion bonding. Continuously energizing the solenoid added a direct-current voltage to the thermal effects in a nonenergized solenoid. No diffusion bonding occurred, and both solenoids were operating satisfactorily at the end of the test. The transformer test was lessened in value by a voltage surge from a power supply. The transformer exhibited electrical continuity after the test, and evaluation will determine the full extent of the failure and what data may still be obtained.

With potassium-lubricated bearings and conventional shaft seals, potassium vapor would be present in the generator rotor cavity (see section on Bearings and Seals). While the solid rotor will not be attacked by the vapor, the insulation in the stator windings will be attacked, and therefore, potassium vapor must be excluded from the stator assembly. The ceramic bore seal shown in figure VIII-31 performs this function. A ceramic bore seal is used because any metallic materials will give eddy current losses. These losses result in heat buildup and a loss of efficiency in the generator.

The ceramic is likely to be beryllia mainly because of its high thermodynamic stability. An added benefit of beryllia is its high thermal conductivity in comparison with other oxides. A high thermal conductivity will reduce temperature differentials and thus diminish the likelihood of cracking the bore seal.

To exclude potassium vapor from the stator totally, other vapor paths to the stator must also be blocked off by attaching the ceramic bore seal to the generator housing and thus indirectly to the bearing and seal housing. This attachment is made by a metal member that must be thin and flexible to allow for thermal expansion mismatches between the ceramic and the generator housings. This construction requires a ceramic-to-metal braze joint that must be leak tight.

This joint is one of the major problems in bore seal construction. A ceramic-to-metal joint is usually made by using an active metal braze, that is, a braze alloy that contains elements which, when molten chemically, react with the surface of the ceramic. This reaction then allows the braze material to wet the surface and thus promotes a good braze joint.

Tests have been conducted on a number of braze alloys. The joint efficiencies range from 60 to 98 percent, that is, the joint strength can be 98 percent as strong as the ceramic beryllia which typically has a modulus of rupture of 25 000 pounds per square inch.

It has been stated that the ceramic-to-metal joints must be leak tight. To check this, assemblies were made with 2-inch-diameter beryllia cylinders fitted with columbium - 1-percent-zirconium end caps. The assemblies tested showed no leakage within the limits of sensitivity of measurement.

PUMPS

The four-loop system shown in figure VIII-1 requires four pumps, one in each loop. For the SNAP-8 program, considerable experience has been gained with motor-driven pumps. Figure VIII-32 shows a motor-driven centrifugal pump described in paper VI. It pumps NaK in the reactor loop of the SNAP-8 system at 1100° F and has accumulated 3000 hours of endurance on a single pump. A pump of this type is thus a candidate for use in three of the four loops. The operating conditions are as follows:

Speed, rpm	5800
Head rise, psi	35
Flow, lb/hr	35 300
Input power, kW	4.6
Overall efficiency, percent	35

In the reactor loop (fig. VIII-1) the fluid temperature is quite high at the pump inlet, about 2000° F. Use of a motor-driven centrifugal pump at this point in the system would require thermal isolation of the motor from the pump in order to limit the motor temperature to the 1100° F for which considerable experience has been gained with electrical materials. Although such thermal isolation has been successful in the SNAP-8 program, a motor-driven pump for this application has not actually been built.

Electromagnetic Pumps

The electromagnetic induction pump is also a candidate for this service. One of the attractive features of the electromagnetic pump is that it is mechanically simple; it has no shaft, bearing, or seal. However, it is not without problems. On the good side of the ledger is the considerable experience obtained to date with electromagnetic pumps in ground installations. They have operated for thousands of hours at fluid temperatures to 2000° F. For example, in one of the corrosion loops, a helical induction pump has circulated sodium at 1990° F for 5000 hours (paper VII, fig. VII-25).

The experience with pumps of this type does not mean, however, that a 2000° F pump is available for use in the reactor loop. The purpose of the pumps to date has been simply to pump liquids at high temperature in a pipe that will contain it. Consequently, the pumps are heavy with much external cooling to eliminate temperature problems. Efficiencies have been typically less than 5 percent, compared with 35 percent for the SNAP-8 mechanical pump just described. What is required, then, is to increase the performance level, while at the same time decreasing the weight.

Figure VIII-33 shows a pump that is designed to have an acceptable level of performance. It is a helical induction pump under development as a boiler feed pump. The operation of this pump is exactly the same as an induction motor. The stator is wound to produce a rotating magnetic field. The core of the pump is an annular pipe containing a helix and liquid potassium, which is electrically conductive. The rotating field causes the potassium to follow a helical path through the duct, in this case from right to left. The pressure of the potassium is continuously increased as it passes through the helical passage within the field of the stator. The stator is thermally insulated from the high-temperature-pump cell. The pitch of the helix is larger on the inlet side of the annulus to avoid cavitation by lowering the velocity at the pump inlet. It should be possible to design such pumps to accept near-boiling fluid at the pump inlet.

The pertinent design point data for the pump under development are as follows:

Head rise, psi	240
Flow, gal/min	33
Temperature, ^{o}F	1000
Efficiency, percent	20

The 20-percent efficiency is a considerable improvement over present high-temperature electromagnetic pumps, but it is still lower than that obtainable from mechanical pumps. It is a trade-off, then, between simplicity and efficiency. The pump is to develop a pressure rise of 240 pounds per square inch with a flow equal to that required for a 300-kilowatt system. Although the design fluid temperature is 1000^{o} F, the pump is to accommodate liquid potassium to 1400^{o} F, and it will be tested at this higher temperature.

In order to increase the temperature level of electromagnetic pumps, use will be made of the advancements in magnetic materials such as those previously described for the generator. Also, the versatility of remotely inducing an electrical force on the conductive potassium makes other types of electromagnetic pumps worth considering. Such studies are underway.

RADIATOR

For the waste-heat rejection system, the liquid coolant from the condenser is pumped to the radiator where it rejects the waste heat by thermal radiation to space. One problem of the radiator is that the pipes through which this liquid flows must be protected against meteoroid penetration. Early meteoroid penetration estimates were based on indirect measurements such as the audible clank or flash of light produced by an impacting meteoroid or the visible light and ionization produced by a meteor in the Earth's atmosphere. A considerable amount of interpretation and speculation was required in order to use these data to predict the amount of meteoroid armor required. Recent data from the Explorer and Pegasus satellites have substantially improved our knowledge of this meteoroid problem. The satellites now yield data in the desired final form, namely, on the frequency of penetration of metallic surfaces, as shown in figure VIII-34. Although the Pegasus data and much of the Explorer data were obtained on aluminum surfaces, they have here been converted to stainless steel by use of the correlating equation of Summers.

The solid line represents a 1963 projection of the data available at that time. The new data lie substantially on this line for thicknesses of a few mils, but for thickness less than 1 mil, the data are below this early prediction. In the range significant for radiator design, the early prediction is still valid.

On the other hand, the ideas of radiator design have been changing (fig. VIII-35). The armored tube and fin is an early approach. Liquid coolant passes through the tubes. The armor surrounding the tubes protects them from meteoroid penetration. Heat from the liquid is conducted through the armor and into the fins. Both the upper and the lower surfaces then radiate this heat to space. If a meteoroid punctures a fin, a very small amount of surface area is lost, and the ability of the radiator to radiate waste heat drops by a negligible amount. On the other hand, puncture of a tube would allow the coolant to leak out, a generally catastrophic event. For this reason, the tubes are heavily armored and spaced far apart. Because tube spacing is limited by the temperature drop resulting from heat conduction through the fins, copper clad with stainless steel is a good material from which to build the fins.

The bumper-fin concept protects the tubes by a meteoroid bumper. A meteoroid that strikes the radiator surface is shattered with the result that only a diffuse spray of smaller particles impinges on the vulnerable tubes. Because this concept employs thermal conduction to carry the heat from the tubes to the radiating surfaces, the problem of temperature drop in the fins is much the same as in the armored tube and fin.

The vapor-chamber-fin concept retains the ability of the bumper-fin to protect the tubes from meteoroid penetration, but it improves the heat-transfer characteristics by adaptation of the ubiquitous heat pipe. Heat is transferred in the following way: The radiator contains a large number of box-like compartments, one of which is shown in figure VIII-35. This box is lined with a wick that is a thin layer of porous material such as wire cloth or sintered metal powder. Enough liquid metal is put into each compartment to saturate the wick. The central cavity contains only the vapor from this liquid metal. Heat from the tubes is conducted to the wick, and thereby some of the liquid in the wick is vaporized. Vapor within this cavity condenses on the two radiating surfaces of the radiator. The condensate thus formed is then transported by capillary forces back to the heating surface, where it is again vaporized. By this convection of metallic vapor and liquid, heat is transferred from the tubes to the radiating surfaces. Because the effective thermal conductivity of the vapor chamber fin is high, not only may the tubes be far apart but also the radiator size may be reduced.

For the vapor-chamber-fin concept, the entire radiator surface is vulnerable to meteoroid penetration. This vulnerability would be a detriment if it were not for the compartmentization of the radiator. A typical radiator might contain of the order of 100 such compartments of which 10 percent might be sacrificed during the mission; in other words, 10 punctures during the mission would result in a 10-percent loss of heat-rejection capacity, a factor easily adjusted for by making the radiator just a bit larger than required. By the combination of improved meteoroid protection and improved lateral heat transfer within the radiator, radiator weight is approximately halved.

Emissive coatings are required for the radiating surfaces. Bare stainless steel radiates only 20 percent as much heat as does a blackbody, therefore, investigations have been made of coatings that have high emissivity. Calcium and iron titanates are the two best coatings to date. Their characteristics are shown in figure VIII-36. The iron titanate has now been endurance tested for $22\frac{1}{2}$ months and the calcium titanate for a full 2 years. The two specimens still have an emissivity of 0.88.

Coatings have also been subjected to additional tests. For example, each test specimen has endured 88 thermal cycles between room temperature and 1350° F. Fatigue specimens have been tested in a standard fatigue machine for as many as 10^{6} stress cycles. For some of the fatigue specimens, the cyclic stress was high enough to fracture the stainless steel. Through all these thermal and stress cycles, the coatings have tenaciously adhered to the metal surfaces, even right up to edge of a fracture. The enduring qualities of these coatings give every indication of their suitability for use on these high-temperature radiators.

CONCLUDING REMARKS

In both this discussion and the discussion in paper VII the technology of potassium-vapor Rankine-cycle turbogenerator power systems has been reviewed, and our work on a variety of constituent problems of these systems has been discussed. On the bases of corrosion and strength, maximum temperatures of 2200° to perhaps 2400° F appear practical (paper VII). Satisfactory thermodynamic data for design of such a powerplant are now available. Adequate information has been obtained on the heat-transfer coefficients and pressure drops of boiling and condensing potassium, and our general knowledge of the problem of boiling stability is advancing. Tolerable turbine blade erosion has been experienced at qualities as low as 93 percent, and investigation of lower values is planned in the near future. Design information on bearings, seals, pumps, and electrical materials is accumulating. The thermal design of radiators is improving, and the meteoroid satellites provide additional confidence that reliable radiators can be designed.

The program at Lewis is now beginning to change in its general character by a shift from the general accumulation of design data into component demonstration. Over the next few years, the major components of such a power system should be ready for testing.

Considerable effort lies ahead in building and testing the first real refractory components typical of advanced Rankine power systems. These components will draw on the fabrication procedures described in paper VII, and special facilities will be required in order to provide the high vacuum specified. Testing of these components and testing of the complete power system will undoubtedly reveal problems presently unknown. In order to obtain the performance and long life required for the high-power missions of the future, extensive design and testing of these advanced components are planned over the next 10 years, drawing on the base of technology described herein.

TABLE VIII-1. - LUBRICANT, SEALS, AND GENERATOR DESIGN

Bearing lubricant	Turbine seal	Generator seals	Generator cavity
Potassium	Potassium - potassium	Potassium - potassium	Potassium vapor
Potassium	Potassium - potassium	Potassium - space	Vacuum
Oil	Potassium - space Oil - space	Oil - space	Vacuum

TABLE VIII-2. - PROPERTIES OF BEARING MATERIALS AT 1200° F

Materials	Coefficient of thermal expansion, $^{\circ}F^{-1}$	Vickers hardness number	1000 hr in potassium	
			Dimensional change, percent	Carbon increase in Cb-1Zr capsule, ppm
Bearing				
TiC-10Cb	4.00×10^{-6}	810	0.008	0
90WC-2CbC-8Mo	2.62	1800	.07	40
74WC-20TaC-6Co	2.97	1020	.014	45
Shaft				
TZM	2.98×10^{-6}	205	-0.04	0
Co-23Ni-1.1Zr-1.8Ti	7.4	----	------	--

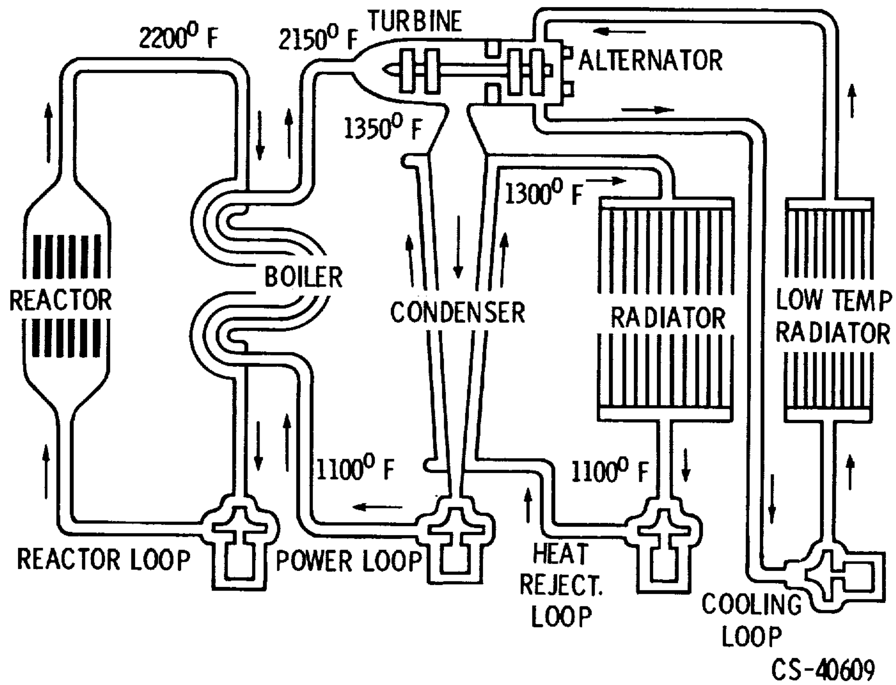

Figure VIII-1. - Potassium Rankine system.

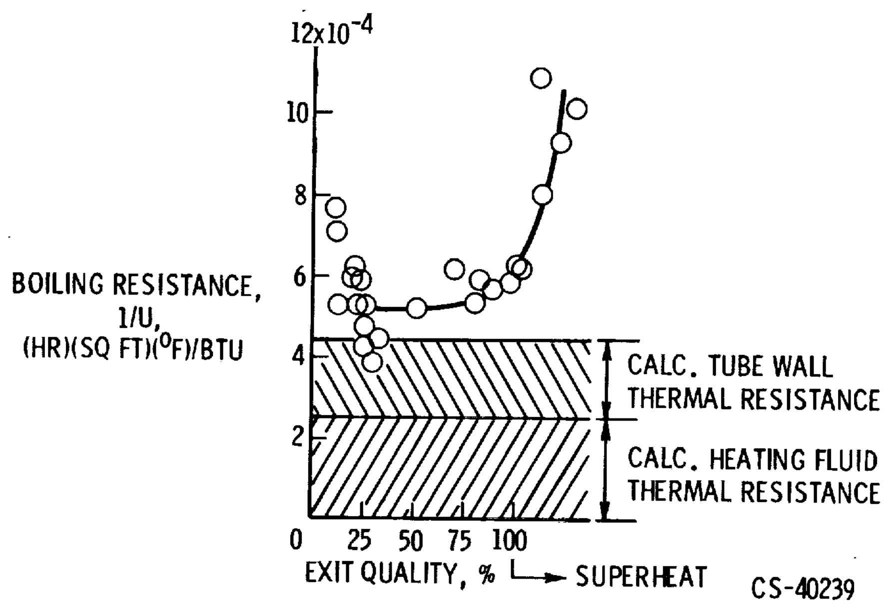

Figure VIII-2. - Overall boiler thermal resistance as function of exit quality.

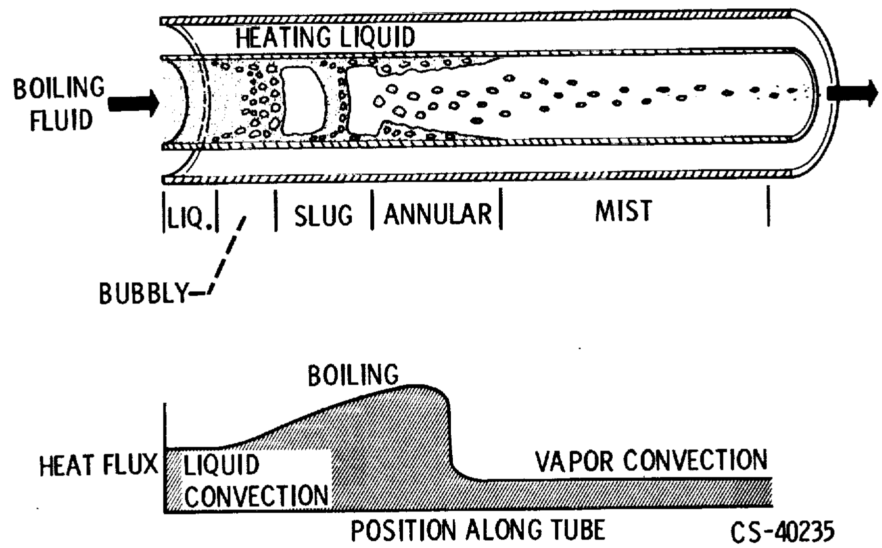

Figure VIII-3. - Two-phase boiling flow regimes.

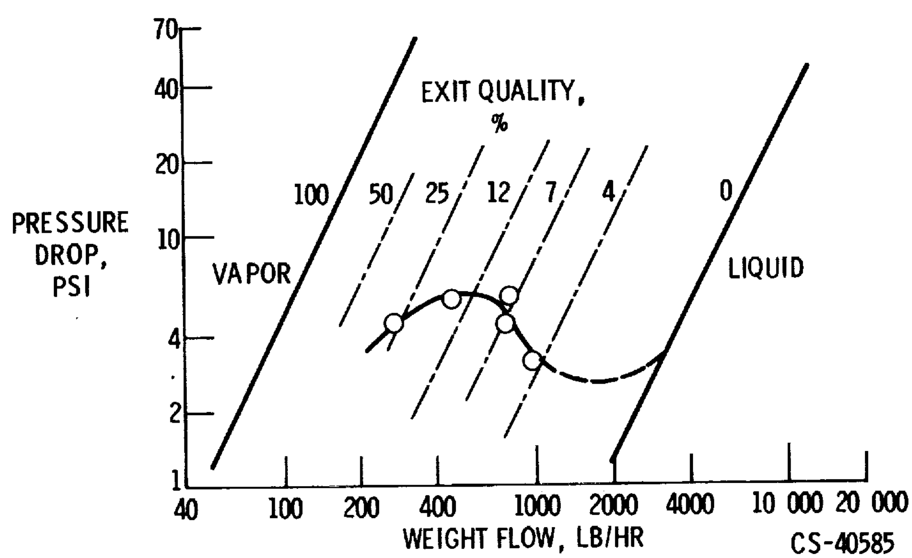

Figure VIII-4. - Boiling pressure drop for sodium.

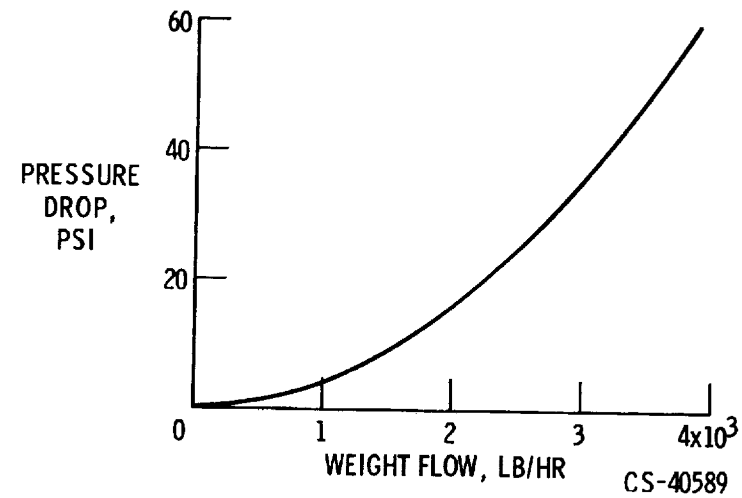

Figure VIII-5. - Orifice pressure drop. Square-law inlet resistance.

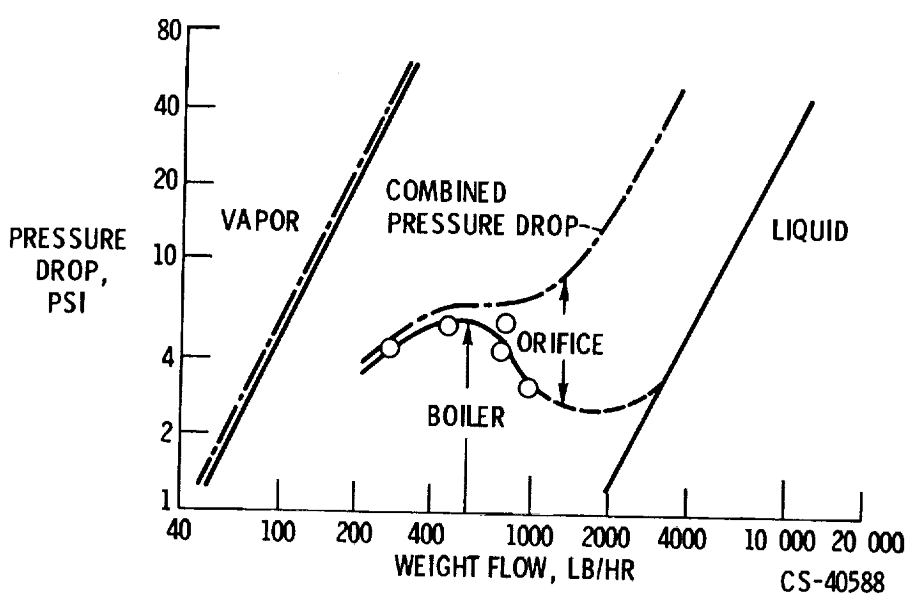

Figure VIII-6. - Boiling pressure drop for sodium.

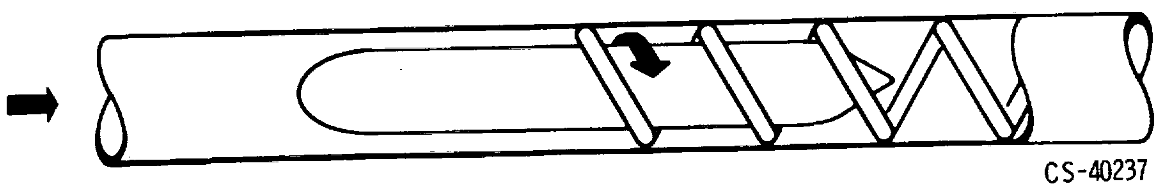

Figure VIII-7. - Center plug and spring boiler inlet insert.

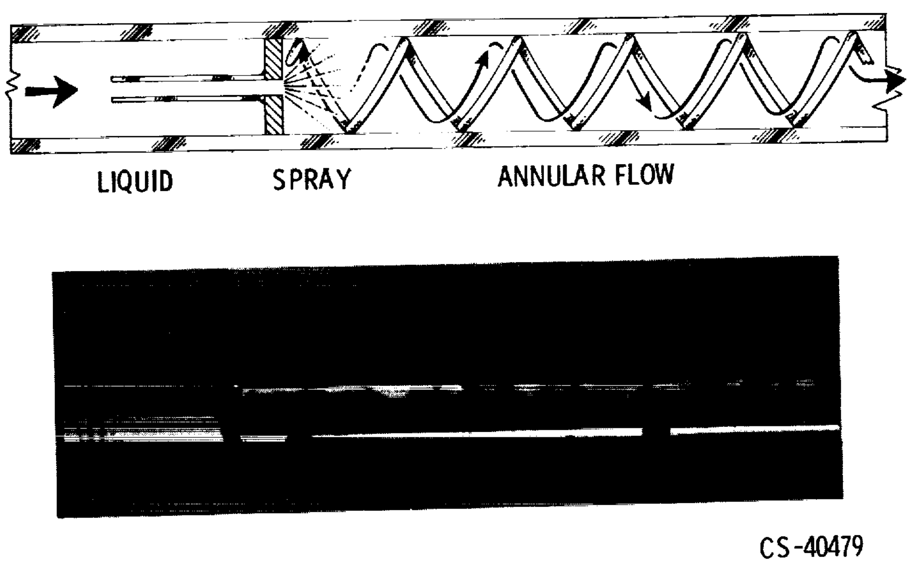

Figure VIII-8. - Center tube and spring boiler tube inlet inserts.

CS-40476

Figure VIII-9. - Closeup of center tube.

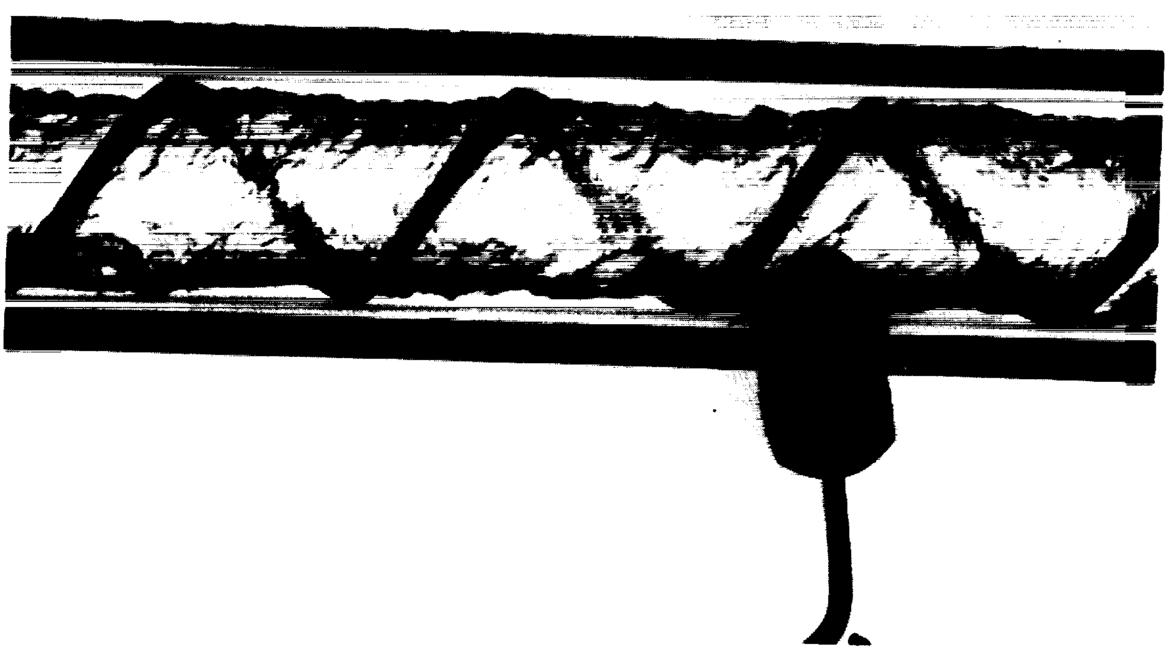

CS-40478

Figure VIII-10. - Closeup of annular region.

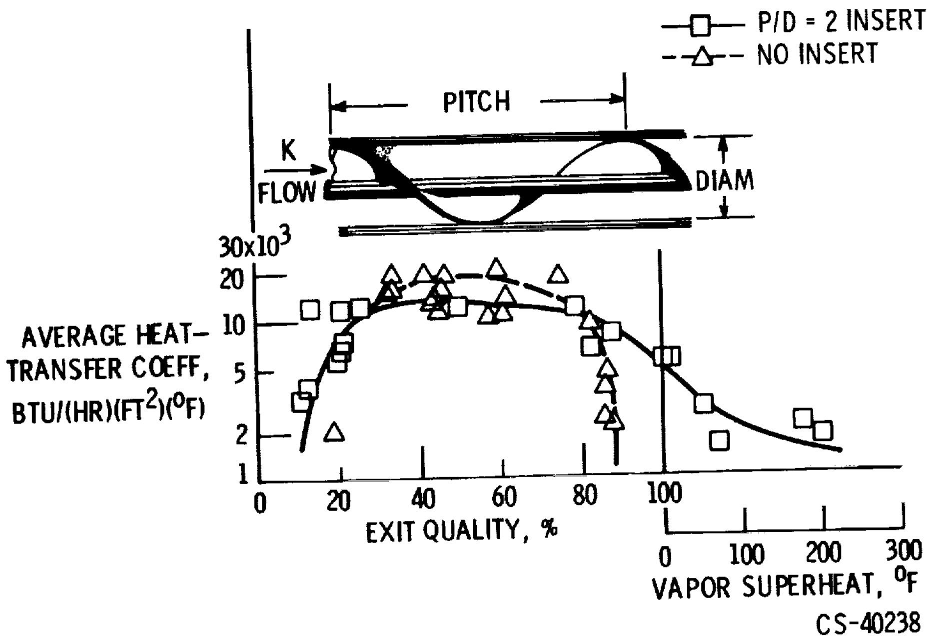

Figure VIII-11. - Boiling potassium heat transfer.

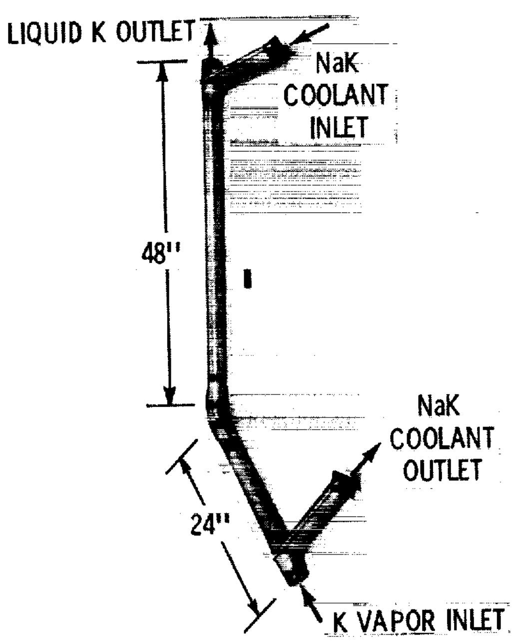

(a) Overall view.

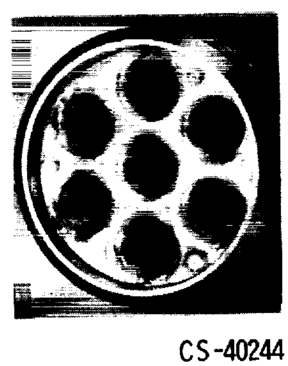

(b) Detail of vapor inlet. Tube outside diameter, 1/2 inch; shell inside diameter, 2 inches; material, 316 stainless steel.

Figure VIII-12. - Seven-tube potassium condenser.

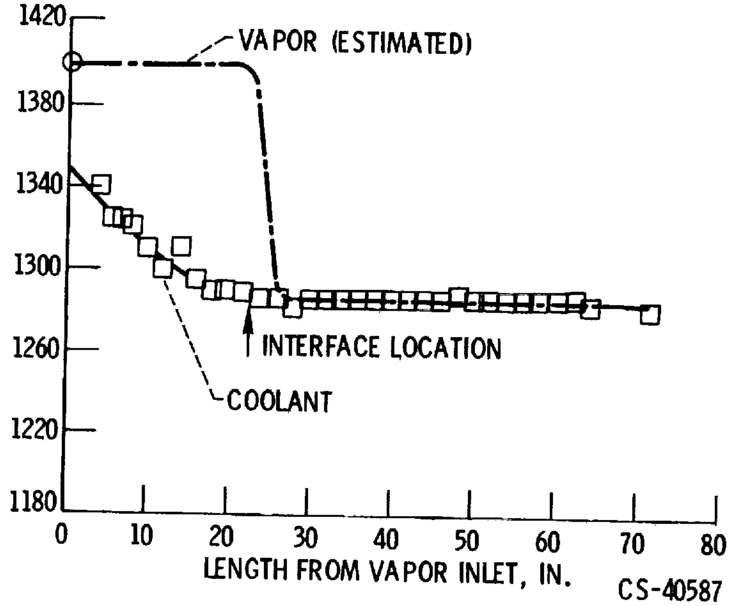

Figure VIII-13. - Condenser temperature profiles.

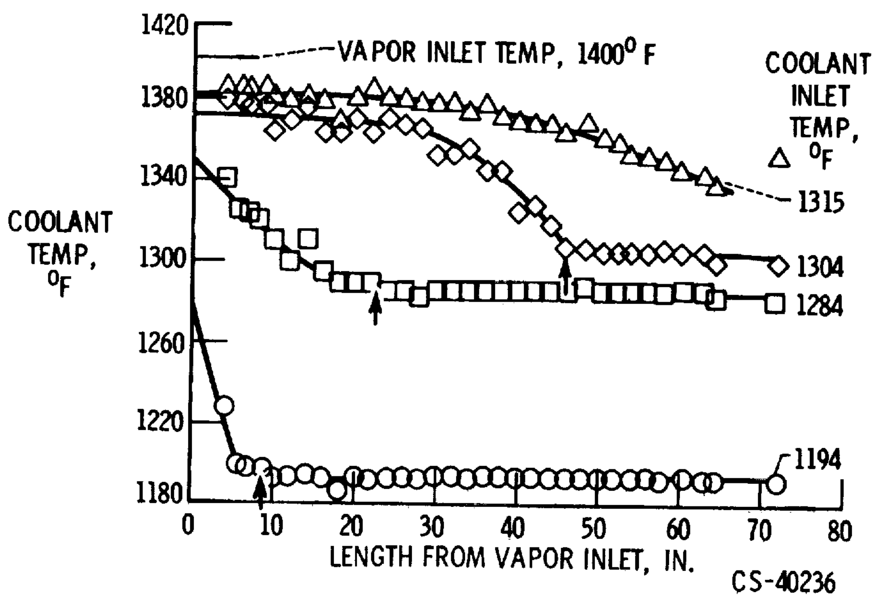

Figure VIII-14. - Seven-tube condenser performance.

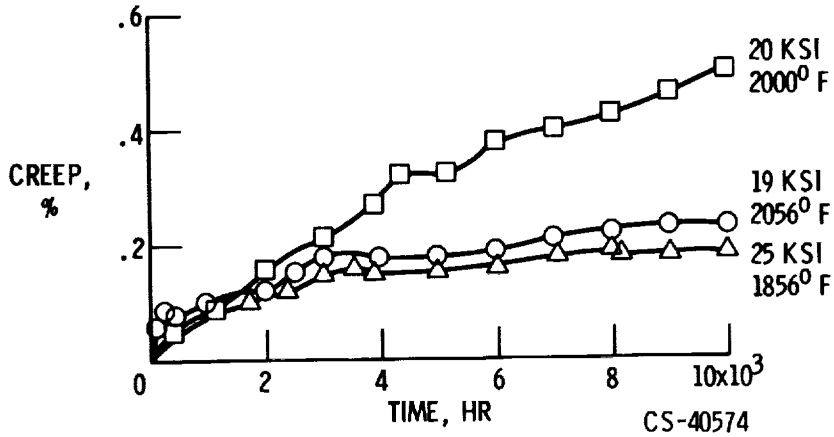

Figure VIII-15. - Creep of TZC (Mo-1.25Ti-0.15Zr-0.12C).

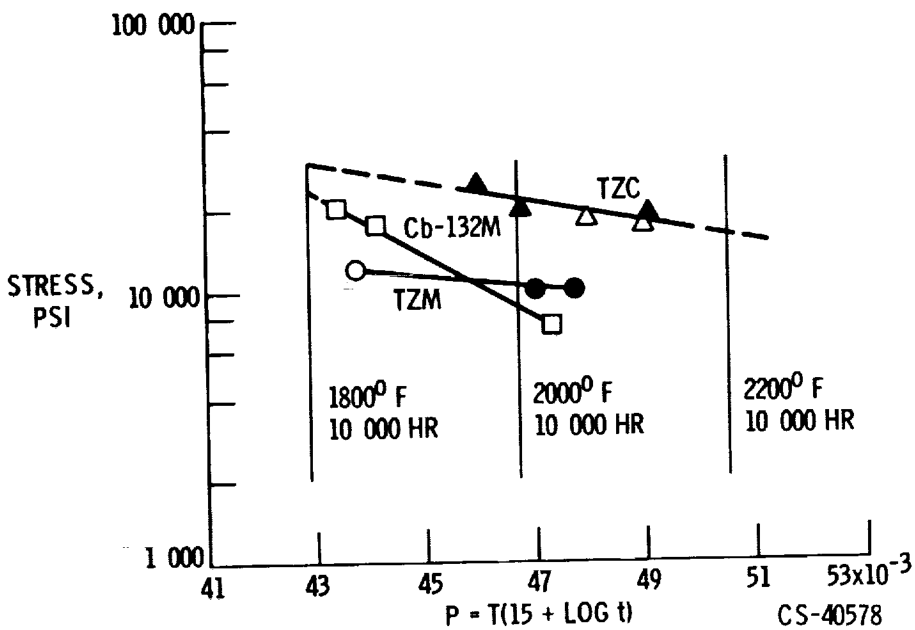

Figure VIII-16. - Strength of turbine alloys for 0.5 percent creep.

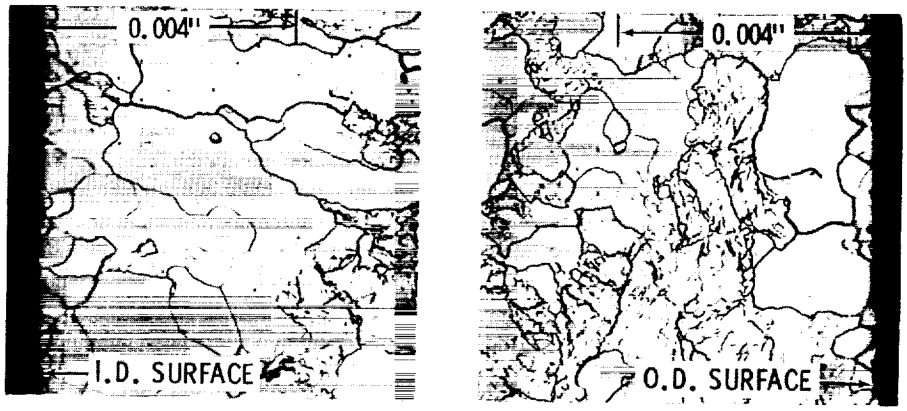

CS-40580

Figure VIII-17. - TZM compatibility with potassium vapor for 5000 hours at 2000° F.

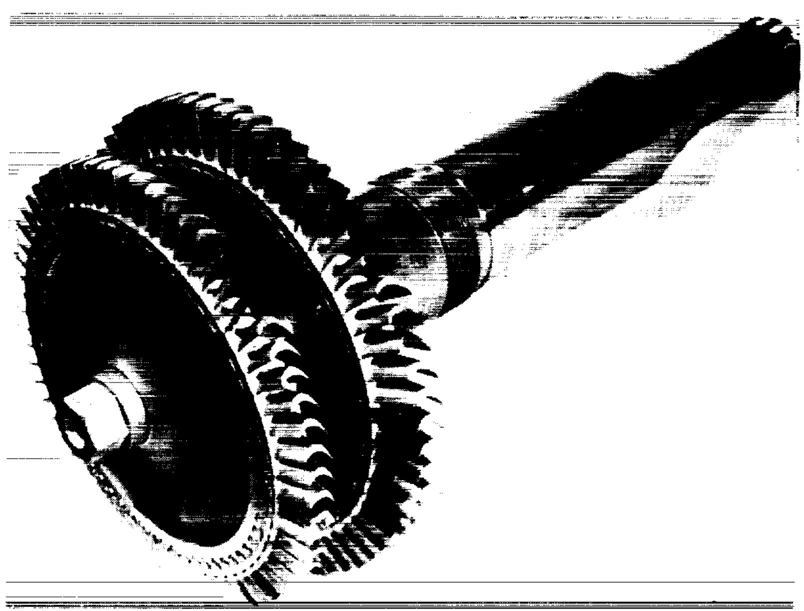

CS-40618

Figure VIII-18. - Potassium turbine rotor.

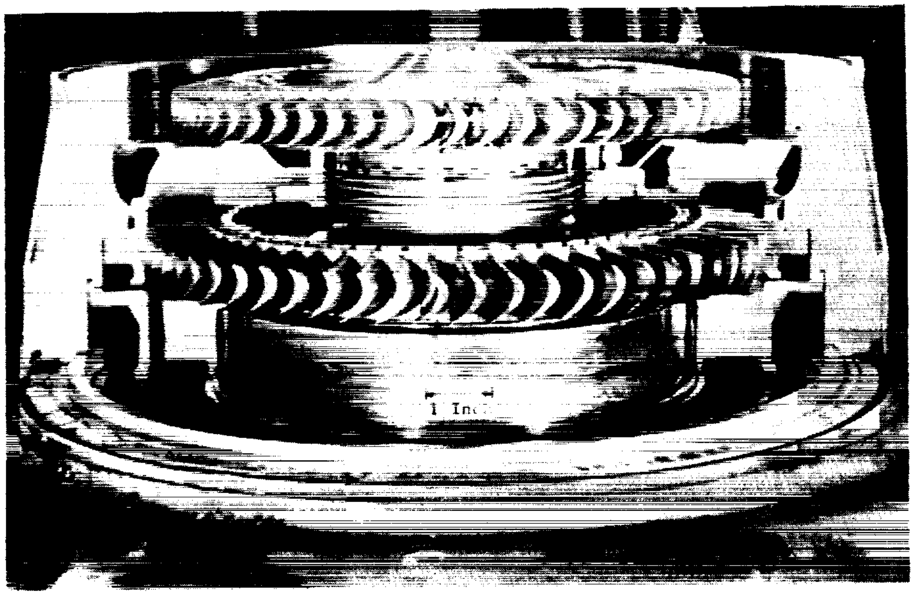

CS-40619

Figure VIII-19. - Turbine partial assembly.

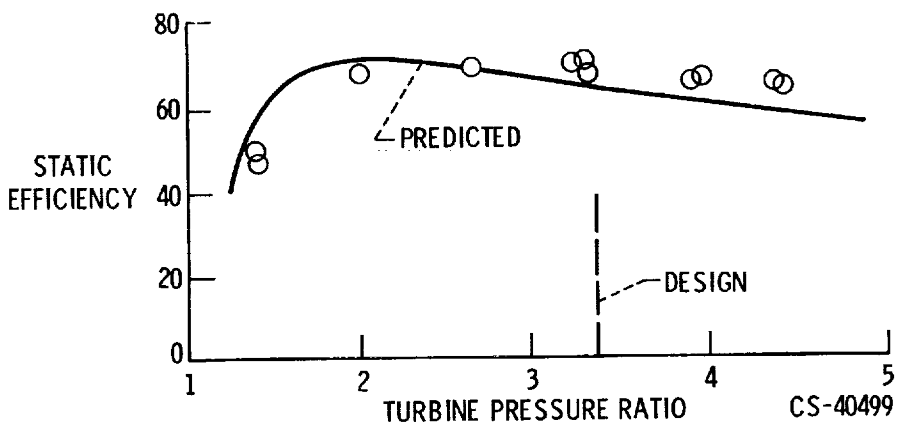

Figure VIII-20. - Two-stage potassium turbine performance. Inlet temperature, 1550° F; quality, 99.5 percent.

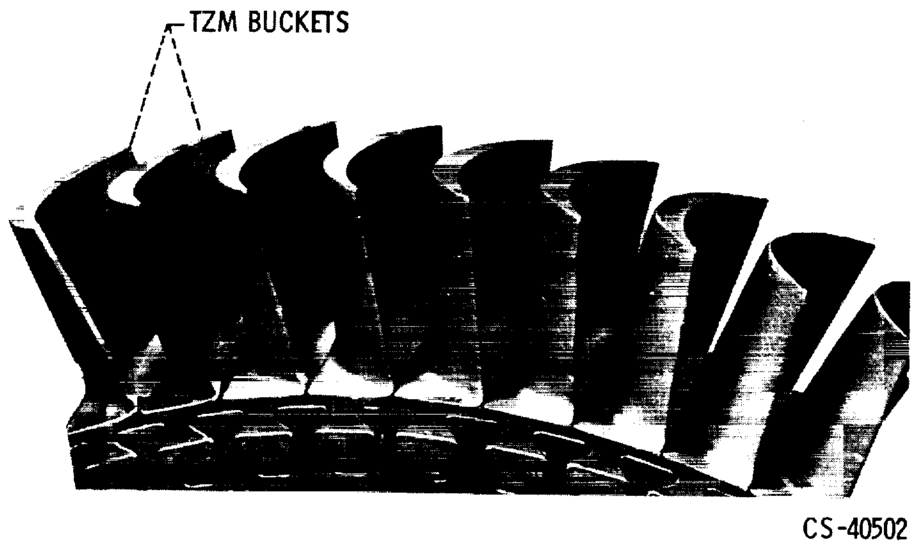

Figure VIII-21. - Second-stage wheel after 2000-hour endurance test.

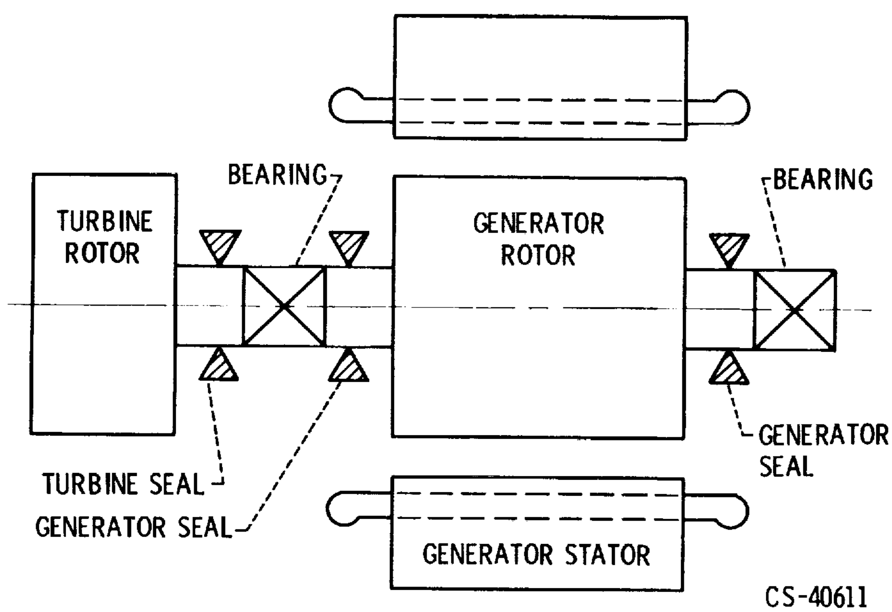

Figure VIII-22. - Turbogenerator bearing-seal arrangement.

CS-40621

Figure VIII-23. - Pivoted-pad-bearing assembly.

CS-40617

Figure VIII-24. - Herringbone groove bearing tested in sodium to 800^0 F.

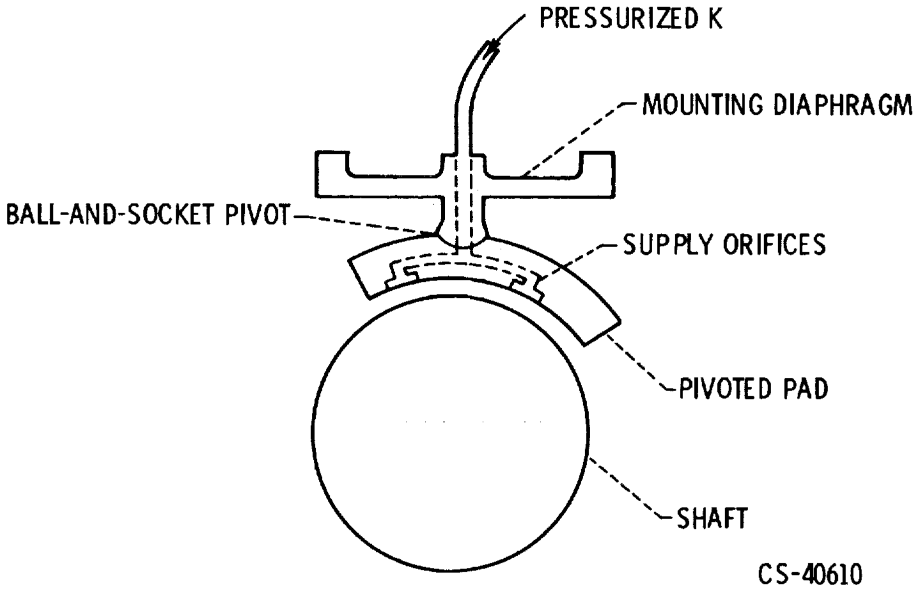

Figure VIII-25. - Mounting arrangement for pivoted-pad bearing.

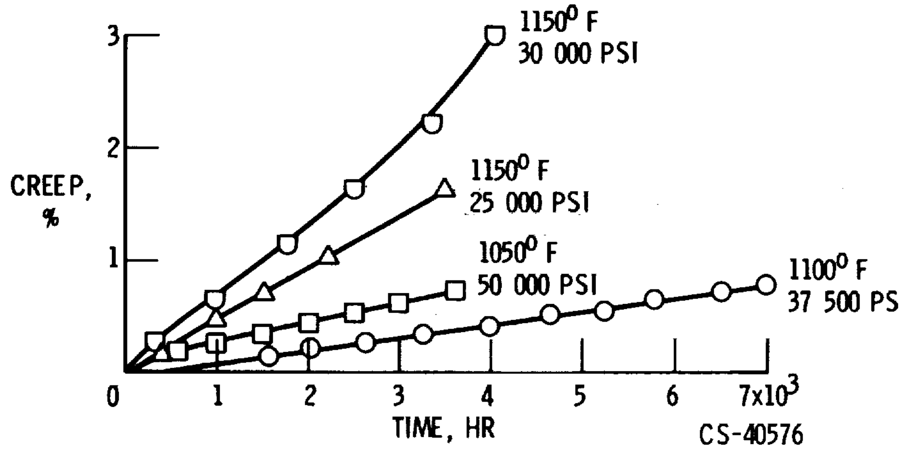

Figure VIII-26. - Creep of Nivco (Co-23Ni-1.1Zr-1.8 Ti).

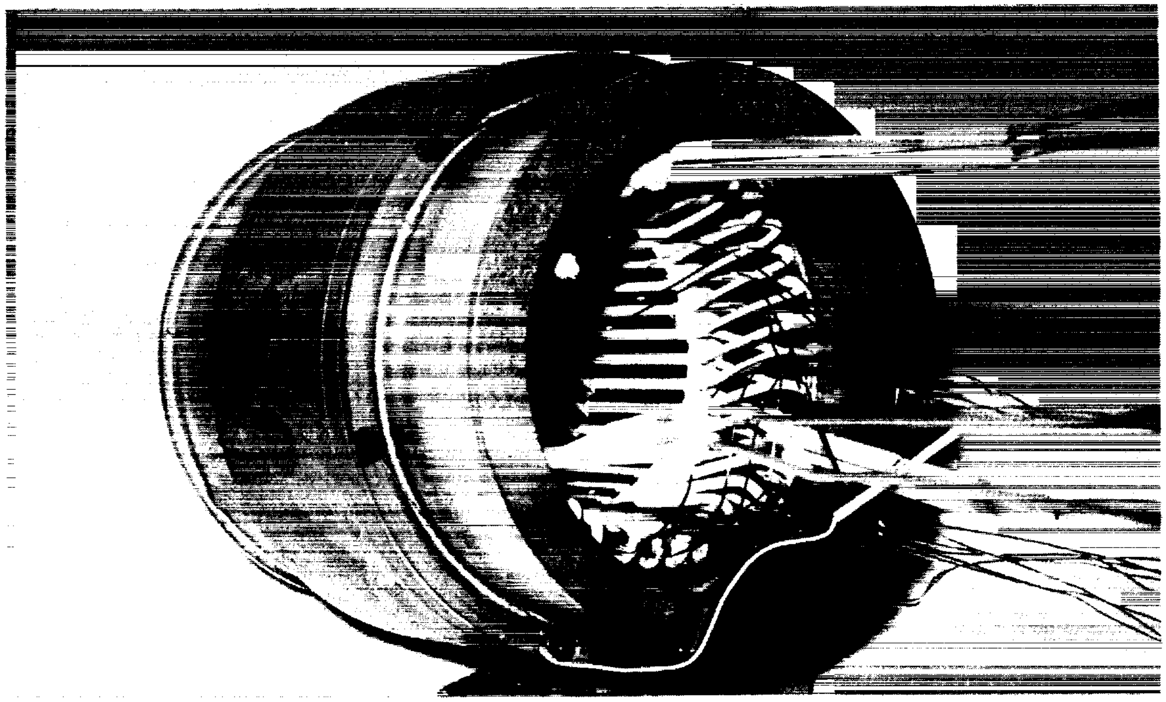

CS-40558

Figure VIII-27. - Statorette assembly tested in vacuum for 5000 hours at 1100^0 F.

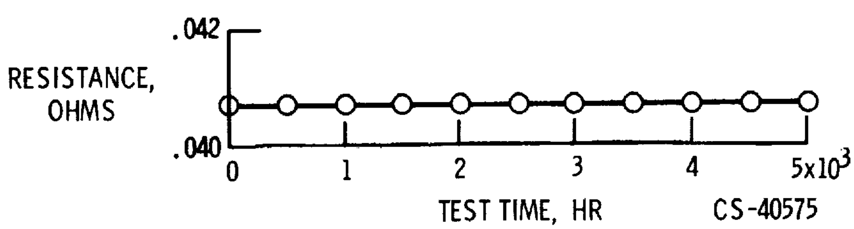

Figure VIII-28. - Conductor resistance at 1100^0 F.

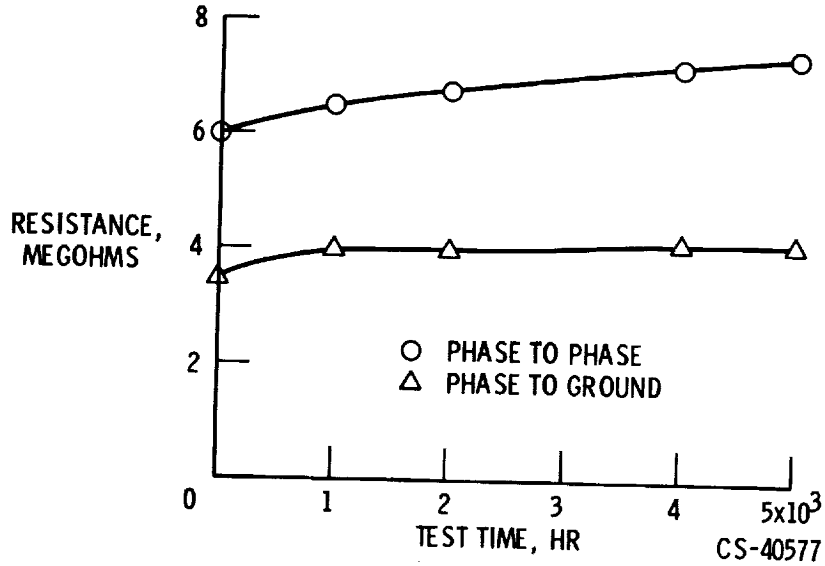

Figure VIII-29. - Statorette insulation resistance at 1100° F.

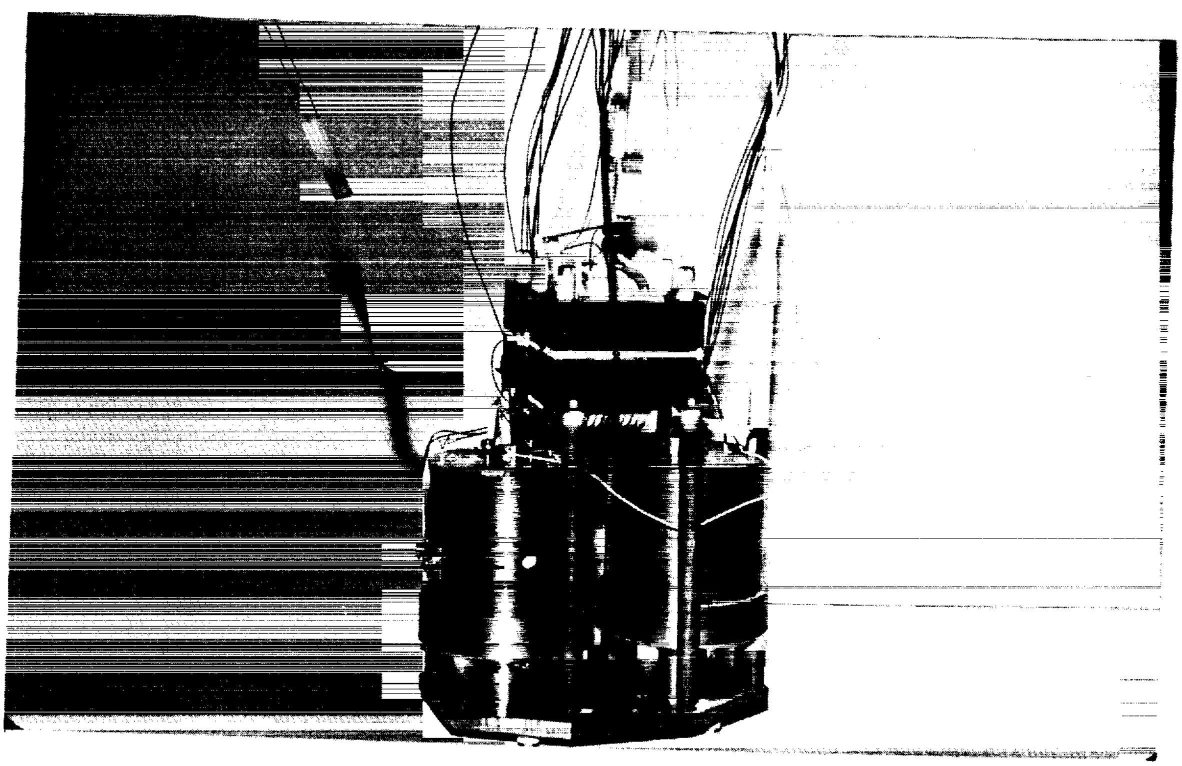

Figure VIII-30. - Solenoid and transformer assembly tested in vacuum for 5000 hours at 1100° F.

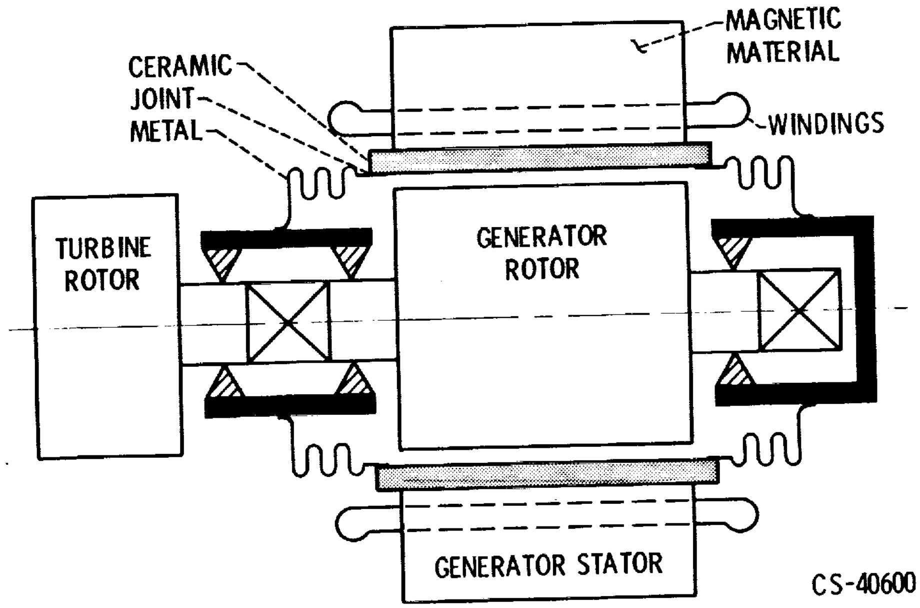

Figure VIII-31. - Generator bore seal.

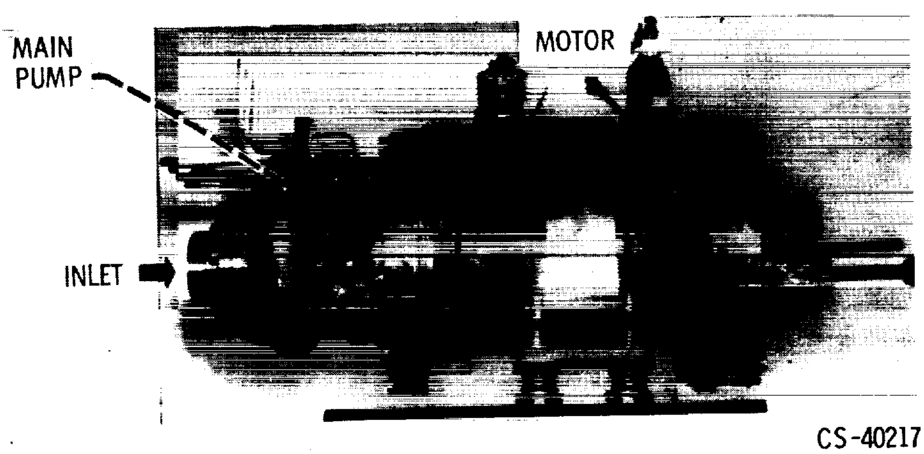

Figure VIII-32. - NaK pump-motor assembly with NaK lubricated, tilting-pad journal and thrust bearings.

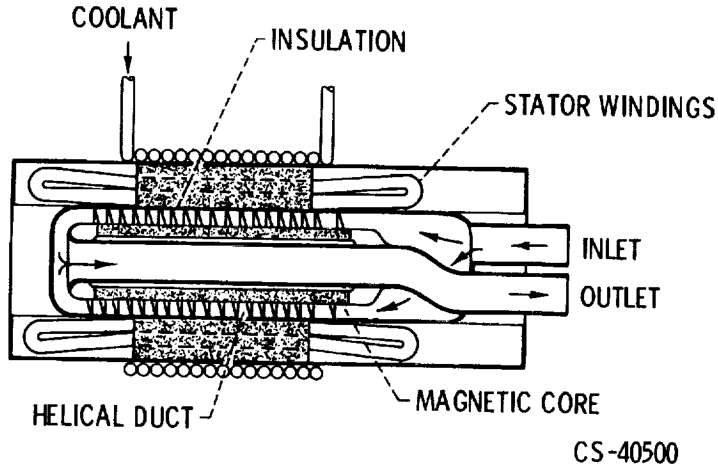

Figure VIII-33. - Electromagnetic helical induction pump.

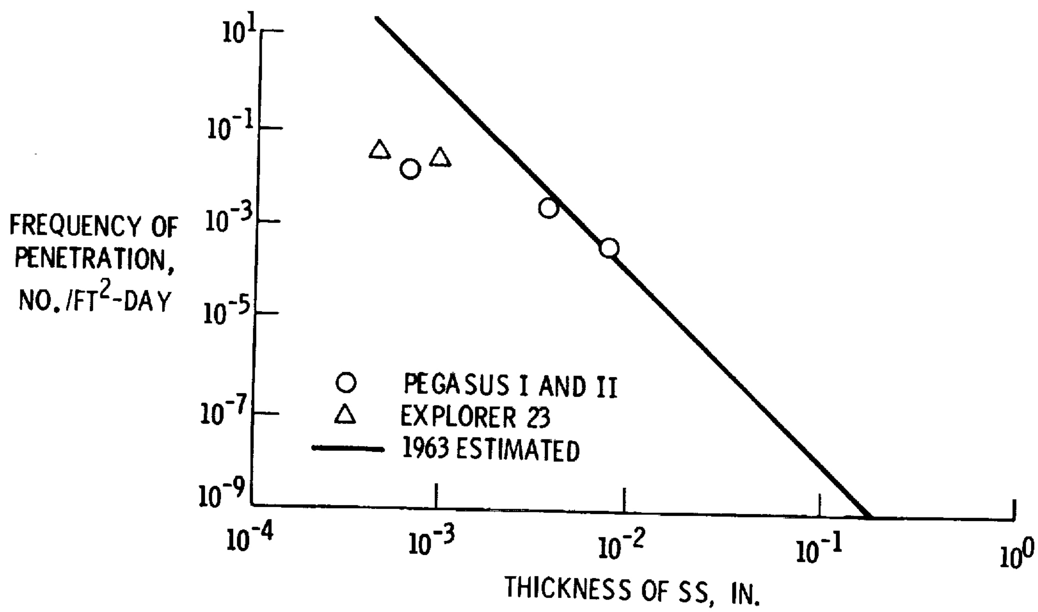

Figure VIII-34. - Meteoroid fluxes for Earth orbit.

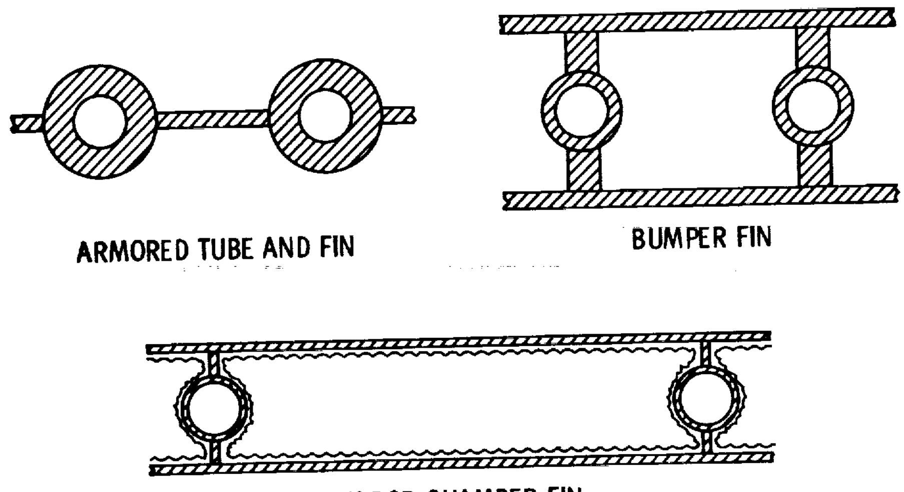

Figure VIII-35. - Radiator concepts.

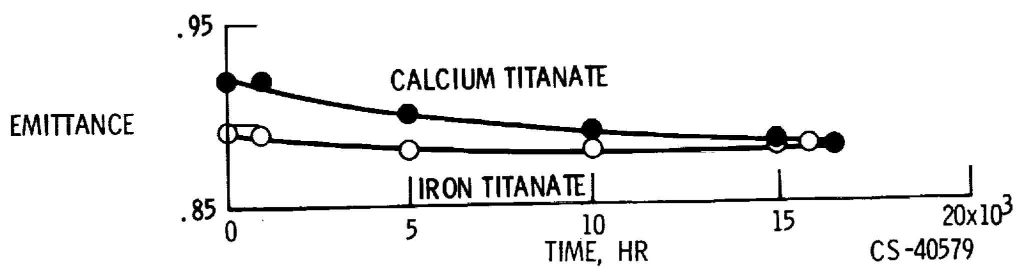

Figure VIII-36. - Endurance test of emissive coatings. Substrate, 310 stainless steel; temperature, 1350° F.